

From the Editors

This issue of the Giovanni News is a special one. It features a dozen images, the first ones selected for the Giovanni Image Hall of Fame. Soon, they will be placed online; this “preview” is especially for subscribers of The Giovanni News.

Many of these images are historical; as Giovanni-4 adds new capability for visualization and analysis, it will be possible to make even better images with the system, perhaps revisiting some of these “classics.” For this inaugural class, images with particular historical interest or scientific impact were selected. We hope that you will find this issue of our newsletter intriguing, and perhaps it will pique some ideas for the use of Giovanni in the future.

Jim Acker and Wainie Youn

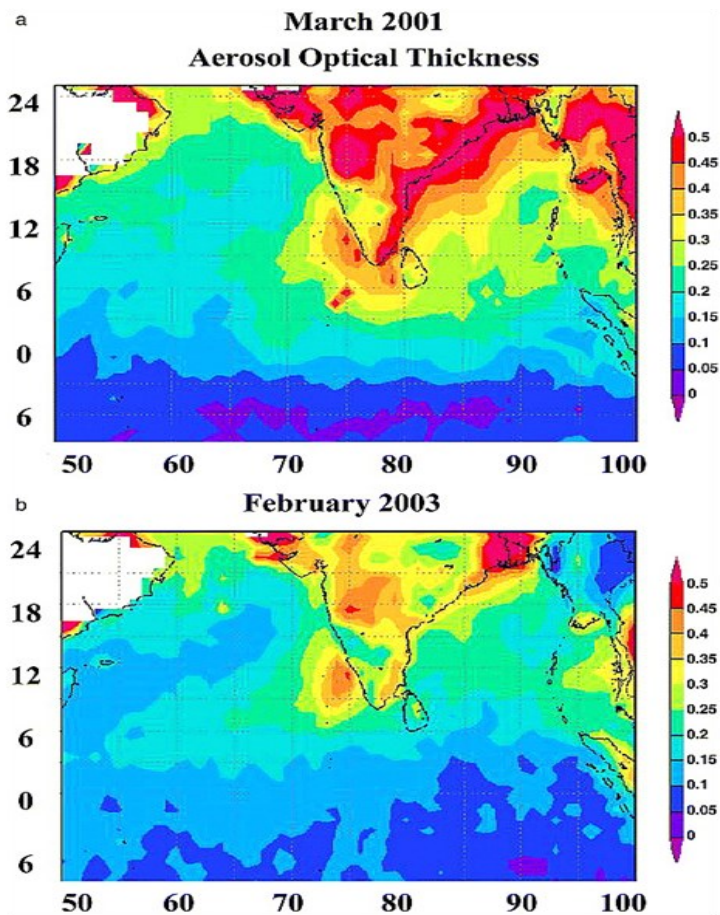
GIOVANNI IMAGE HALL OF FAME

1. Regional distribution of aerosol optical depth (550 nm) during (a) March 2001 and (b) February 2003 (<http://lake.nascom.nasa.gov/movas>)

This was the first Giovanni image to appear in a peer-reviewed research journal. The article in which it appeared was the following:

Vinoj, V., Babu, S., Sateesh, S., Moorthy, K., & Kaufman, Y. (2004). Radiative forcing by aerosols over the Bay of Bengal region derived from shipborne, island-based, and satellite (Moderate-Resolution Imaging Spectroradiometer) observations. *Journal of Geophysical Research*, **109**, D05203, doi:10.1029/2003JD004329.

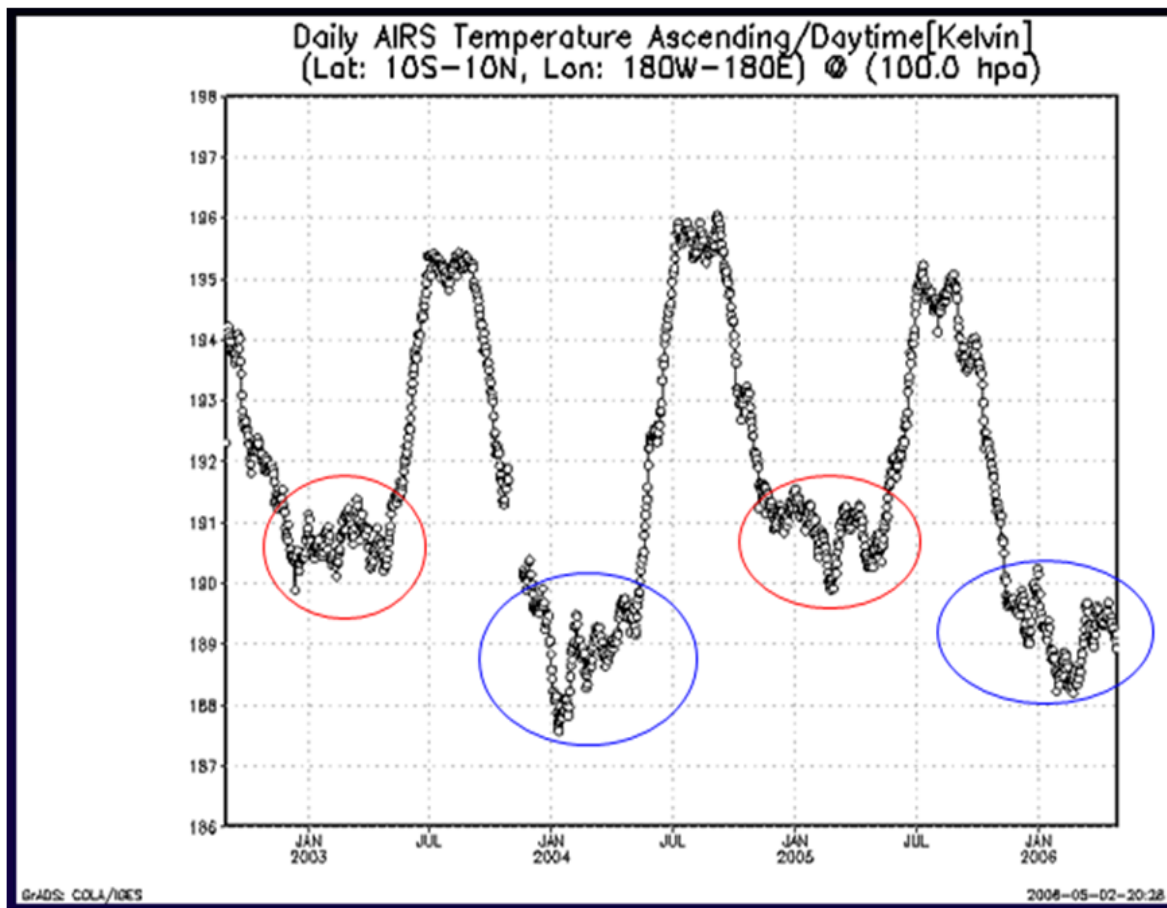
Co-author Yoram J. Kaufman was a leading atmospheric scientist, specializing in atmospheric aerosols, at Goddard Space Flight Center. Kaufman and Greg Leptoukh conceived of the Giovanni system, because Kaufman wanted to be able to analyze data without having to do any computer programming. Kaufman, who died on May 31, 2006 from injuries he received in a bicycling accident, was the Project Scientist for the Terra mission for four years. He received both the NASA GSFC William Nordberg Award for Earth Science and the NASA Medal for Exceptional Scientific Achievement.



2.

The Quasi-Biennial Oscillation

(plotted by Greg Leptoukh)



Dr. Greg Leptoukh, whom many have called “The Father of Giovanni,” plotted this representation of the Quasi-Biennial Oscillation (QBO) for a poster about Giovanni. The daily atmospheric temperature data are from the Atmospheric Infrared Sounder (AIRS) instrument on the Aqua satellite. The temperature data shown here are for the 100 hectoPascal pressure level. (Greg Leptoukh passed away on January 12, 2012.)

The Quasi-Biennial Oscillation is “a quasi-periodic wave-driven zonal mean wind reversal that dominates the low-frequency variability of the lower equatorial stratosphere (3 to 100 hPa) and affects a variety of extratropical phenomena, including the strength and stability of the winter polar vortex” – Intergovernmental Panel on Climate Change Fourth Assessment Report (2007).

3. *Eos* article dust storm montage

The need for an article about Giovanni – that could be referenced by scientists who used Giovanni in studies published in peer-reviewed science journals – was the main reason for such an article, published in the American Geophysical Union’s weekly newspaper *Eos*. A moderate dust storm streaming off the north African coast directly over Dakar, Senegal, provided an ideal case study to show off four of Giovanni’s capabilities: Data map, Hovmöller plot, time-series, and vertical profile.

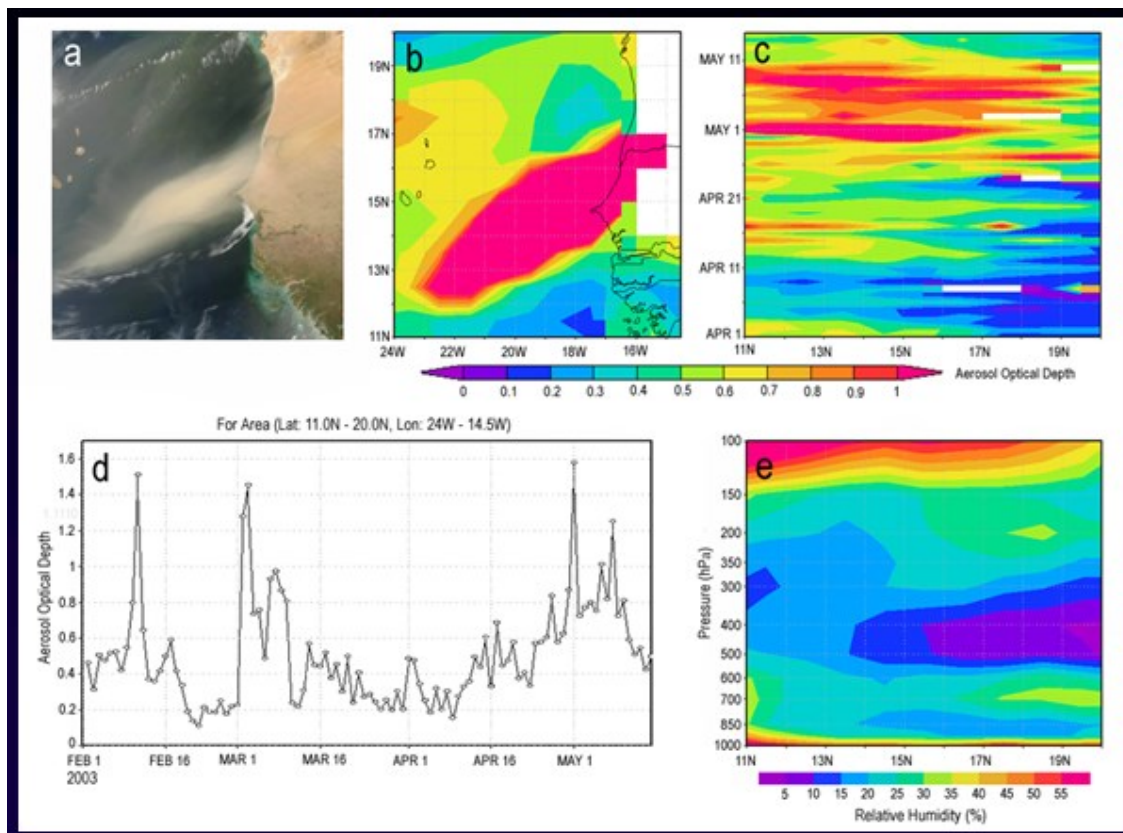


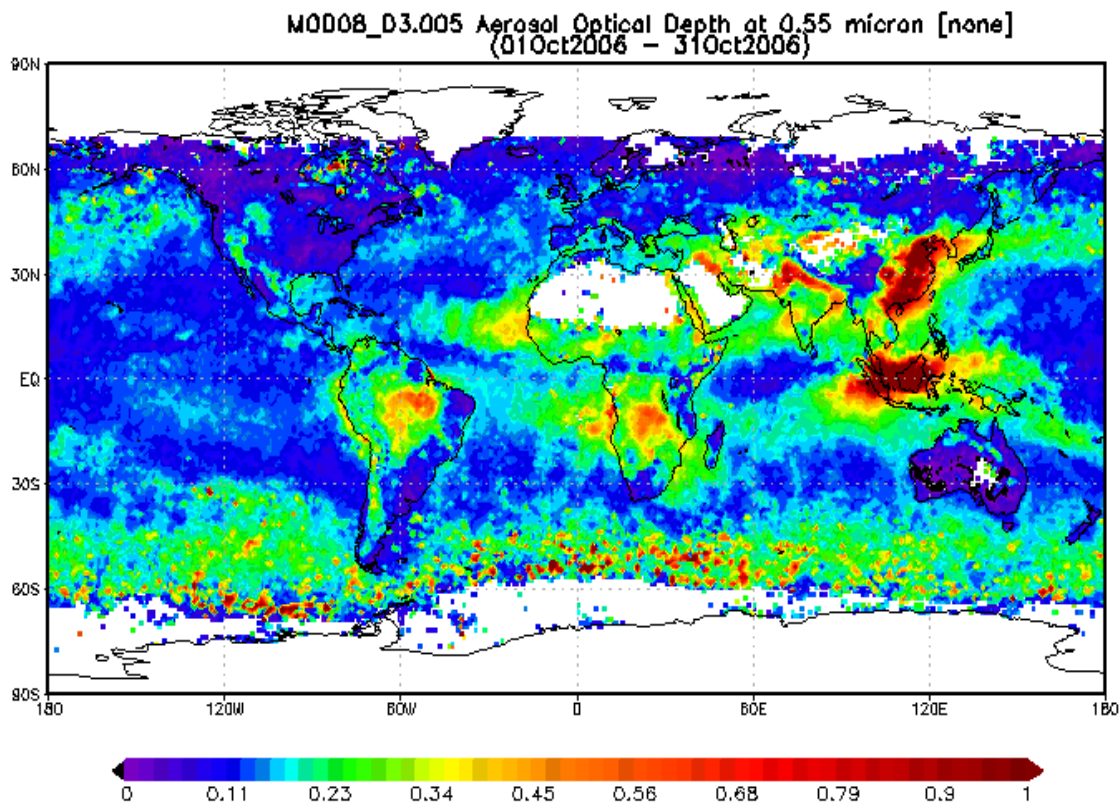
Fig. 1. (a) MODIS-Aqua image of Saharan dust storm, 30 April 2003. The Cape Verde islands are at left. Dakar, Senegal, is the hook-shaped peninsula under the dust cloud on the coast, and coastal wetlands of Gambia and Guinea-Bissau are at the bottom, (b) Aerosol optical depth (AOD) map of this event from MODIS-Terra data, (c) Hovmöller latitude versus time plot of MODIS-Terra AOD for late April and early May 2003, showing the initial southern direction of dust movement, (d) MODIS-Terra AOD time series for February to mid-May 2003, showing that another large dust storm occurred in February, (e) Atmospheric Infrared Sounder (AIRS) relative humidity atmospheric profile plotted against latitude, showing the penetration of dry Saharan air with the dust storm over the Atlantic Ocean.

Acker, J.G. and Leptoukh, G. (2007). Online analysis enhances use of NASA Earth science data. *Eos, Transactions American Geophysical Union*, **88(2)**, pages 14 and 17.

4.

Sources of biomass burning aerosols

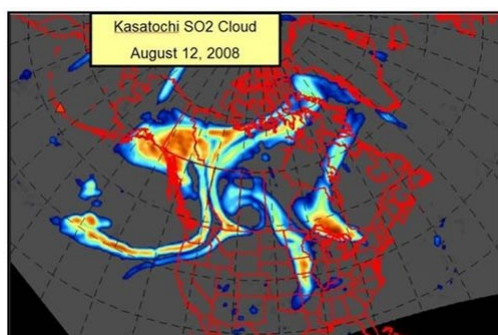
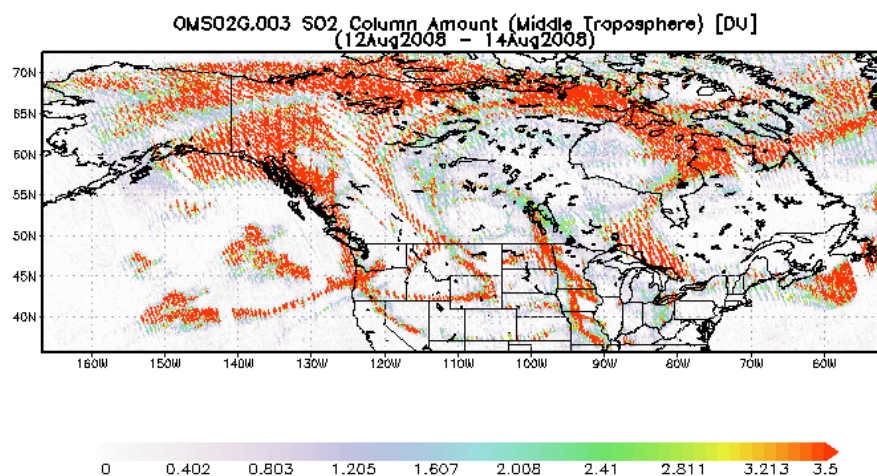
MODIS-Terra aerosol optical depth for October 2006: This image shows one of the most intense aerosol plumes ever to emanate from southeast Asia, mainly Indonesia.



This image, created by Keith Potts of Australia, shows, in addition to the thick biomass burning smoke plume from Indonesia, several other manifestations of atmospheric aerosols and pollution aerosols. Biomass burning aerosols are visible over the Amazon rain forest of South America and the southern Africa rain forest. Pollution aerosols are evident north of the Persian Gulf, along the Himalayan front range in India and Pakistan and extending southward into Bangladesh, and over much of China. The high aerosol optical index over China is due to both biomass burning and emissions from coal-fired power plants. Potts noted that there are eight major continental-scale sources of atmospheric aerosols that appear with varying intensity annually: South America, West Africa, Chad and Mali, Central Africa, the Middle East, India & Pakistan, Southeast Asia, and East Asia.

5. The Kasatochi eruption sulfur dioxide plume

The small Aleutian island of Kasatochi was one of many small and quiet volcanic islands in the chain until August of 2008, when it abruptly awakened and produced a short-lived and powerful eruption. No humans were killed, but two ornithologists on the island had a very close call. The sulfur dioxide (SO₂) from the eruption was thrown into the upper atmosphere, where it was captured by high level winds, which twisted and contorted the SO₂ cloud above much of North America. The Ozone Measuring Instrument (OMI) data in the Giovanni L2G (Level 2 Gridded) portal were plotted for the period August 12-14, showing the various lobes of the aerosol cloud. (This image was used in the first Giovanni brochure.) It's always nice to be able to check one's work: Simon Carn of UMBC produced a similar plot for August 12 with OMI SO₂ data that showed a very similar distribution of volcanic aerosols.



Composite satellite image from August 12 showing the sulfur dioxide cloud produced by the August 7 eruption of Kasatochi. This cloud circled the northern hemisphere between 10,700 to 13,700 meters above sea level. Colors represent relative amounts of gas with dark orange being the highest and dark blue the lowest. These data are from NASA's EOS-Aura satellite and its Ozone Monitoring Instrument (OMI), courtesy of Dr. Simon Carn, University of Maryland, Baltimore County.

6. The Kasatochi eruption phytoplankton bloom

Brief disruptions to air travel, the new steaming caldera, and the SO₂ cloud were not the end of the Kasatochi story. The big blast also deposited a very large amount of volcanic ash in a very short time on the surface of the Pacific Ocean. For several years since the 1990s, oceanographers had tested the “iron hypothesis” of ocean phytoplankton growth, which postulates that iron is a limiting nutrient for the growth of phytoplankton in many parts of the ocean, that is, if iron is not available in sufficient amounts in seawater, phytoplankton can’t grow well. Deliberate releases of iron into the ocean had induced blooms, but Kasatochi provided a natural experimental test.

Researchers observed the occurrence of phytoplankton blooms in the northern Pacific Ocean, just a couple of weeks after the Kasatochi eruption (unusual for August), and attributed it to the deposition of iron-rich volcanic ash on the ocean surface. Giovanni was used to make a time-series of phytoplankton chlorophyll concentrations. (The paper by Hamme et al. (2010) also marked the first time that a publication of a study using Giovanni was discovered via a tweet on Twitter and then downloaded.)

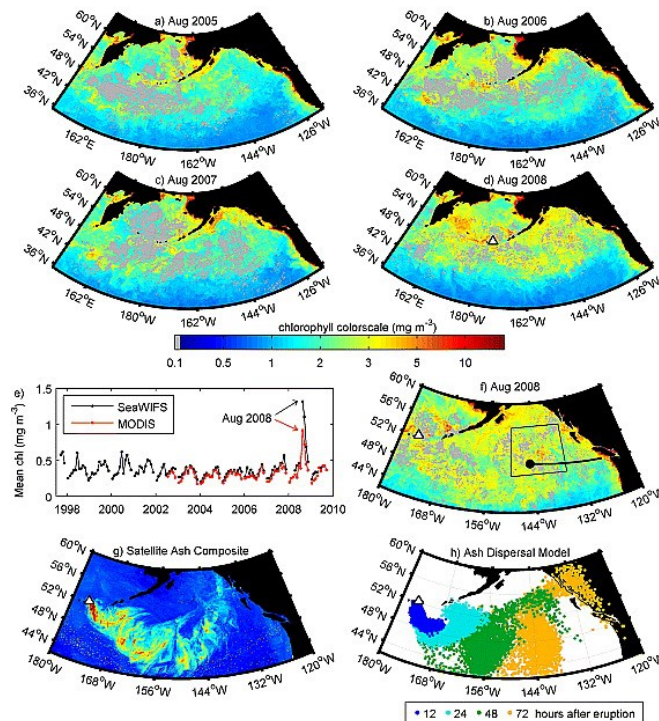


Figure 1. (a–d) North Pacific MODIS monthly-averaged surface chlorophyll in August 2005, 2006, 2007, 2008. (e) Time series of monthly mean chlorophyll averaged over box shown in Figure 1f. (f) Zoom on subarctic NE Pacific MODIS August 2008 chlorophyll, same spatial grid as Figures 1g and 1h. Box shows area of time series averaging. Line from coast shows mid-August cruise track. Point at end of line shows Station P. White triangles show Kasatochi volcano. (g) Composite of most intense satellite detections of airborne ash from the Kasatochi eruption. (h) Particle locations at 0–10,000 m altitude from ash dispersal model at 12, 24, 48, and 72 hours after the start of the Kasatochi eruption.

Hamme, R.C., Webley, P.W., Crawford, W.R., Whitney, F.A., DeGrandpre, M.D., Emerson, S.R., Eriksen, C.C., Giesbrecht, K.E., Gower, J.F.R., Kavanaugh, M.T., Peña, M.A., Sabine, C.L., Batten, S.D., Coogan, L.A., Grundle, D.S., and Lockwood, D. (2010). Volcanic ash fuels anomalous plankton bloom in subarctic northeast Pacific. *Geophysical Research Letters*, **37**, L19604, doi:10.1029/2010GL044629.

7. Flash flood early warning system for Egypt

Cools et al. describe a warning system for flash floods over parts of Egypt’s Sinai Peninsula. Rain events here are understandably rare, as this is an arid region; for the period 1979 -2010, only 20 significant rain events were measured. Yet, flash flood risks from such rain events are real; nine of these events resulted in flash floods. By characterizing prior events that resulted in floods (which is how Giovanni’s 3-hourly Tropical Rainfall Measuring Mission data portal was utilized for this data-poor region), a model was developed that indicated the threshold for sufficient precipitation to cause a flash flood. Though the model didn’t get the estimates of the flash flood depth and duration quite right, the model successfully forecast flash floods for rain events that occurred on October 24, 2008 and January 17-18, 2010. The bottom right panel shows the rain event that caused the January 2010 flash flood.

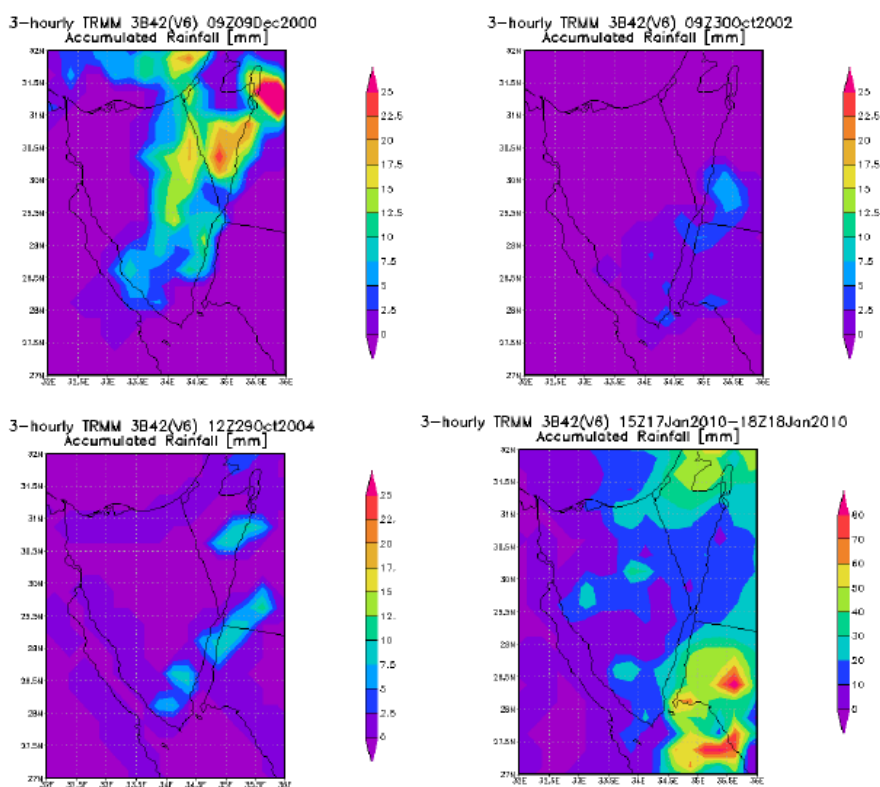


Fig. 7. Selection of 3-hourly rainfall estimates from TRMM for the events in December 2000, October 2002, October 2004, and January 2010. Images have been extracted with NASA’s Giovanni (<http://giovanni.gsfc.nasa.gov>).

Cools, J., Vanderkimpfen, P., El Afandi, G., Abdelkhalek, A., Fockedey, S., El Sammany, M., Abdallah, G., El Bihery, M., Bauwens, W., and Huygens, M. (2012). An early warning system for flash floods in hyper-arid Egypt. *Natural Hazards and Earth System Sciences*, **12**, 443-457.

8. Fire pixel counts for Mount Batchelor aerosols

Image 4 in this inaugural class of Giovanni Hall of Fame images showed sources of biomass burning aerosols in the atmosphere. One “burning” question about these aerosols is how far their effects extend. To examine these effects, Fischer et al. studied the concentration of a biomass burning byproduct (peroxyacetyl nitrate or PAN) collected in air samples taken at Mount Batchelor in Oregon. PAN is important because it is a chemical precursor to tropospheric ozone (O_3), which degrades air quality in urban regions and can enhance haze in rural regions like Mount Batchelor. Giovanni was used with the MODIS fire pixel count data product to correlate the occurrence of fires with the measurements of PAN in the spring at Mount Batchelor. Black-and-white and remarkably simple, this plot shows exactly what the authors want it to show.

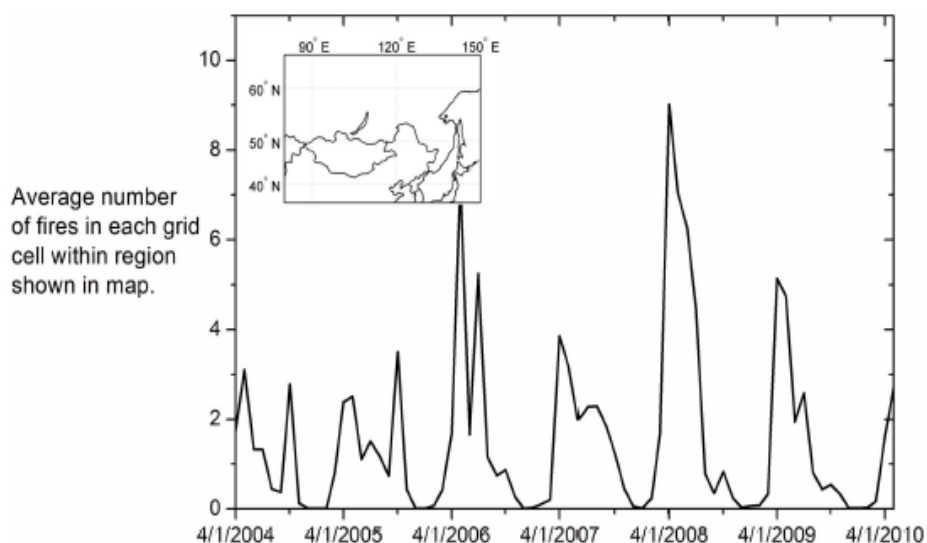


Fig. 3. Monthly average number of fires in each grid cell in region bounded by 35° N–65° N and 80° E–150° E (shown in inset map). Fires peak in this region in spring. There was an early and very strong fire source in this region in April and May 2008 due to early snow melt. Data used in this figure were retrieved from the Giovanni online data system, developed and maintained by the NASA GES DISC Northern Eurasia Earth Science Partnership Initiative (http://gdata1.sci.gsfc.nasa.gov/daac-bin/G3/gui.cgi?instance_id=neespi) (Acker and Leptoukh, 2007).

Fischer, E.V., Jaffe, D.A., and Weatherhead, E.C. (2011). Free tropospheric peroxyacetyl nitrate (PAN) and ozone at Mount Batchelor: causes of variability and timescale for trend detection. *Atmospheric Chemistry and Physics*, **11**, 5641–5654, doi:10.5194/acp-11-5641-2011

9. Sea surface temperature of Hudson Bay

Climate change is expected to have many different effects in the polar regions. One of the most hotly-debated issues is the effect that climate change will have on large organisms like caribous, walrus, and polar bears in the Arctic. The Hudson Bay population of polar bears comes under the most scientific scrutiny, because the sea ice cover of Hudson Bay has been changing very significantly, apparently causing polar bears in this region to wait longer and longer in the autumn before they can venture onto the sea ice to hunt.

In a chapter for a book on the top predators in the Hudson Bay ecosystem, the average summer sea surface temperature (SST) in 2006 for this vital body of water was illustrated using SST data from the Moderate Resolution Imaging Spectroradiometer (MODIS). This striking image also shows that warmer waters are found near the coast and warm land surface. The chapter describes the variety of processes that can affect water temperature and sea ice formation. Another Giovanni image in the chapter shows average summer chlorophyll concentrations in Hudson Bay.

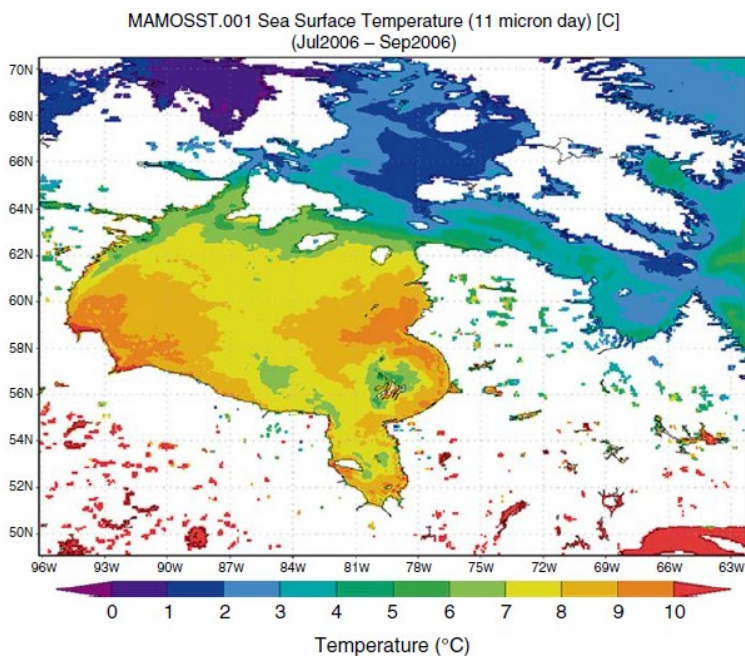


Fig. 8 Summer (July–September) sea surface temperature in 2006 (Prepared using the Giovanni online data system, developed and maintained by the NASA Goddard Earth Sciences (GES) Data and Information Services Center (DISC))

Stewart, D.B. and Barber, D.G. (2010). *The ocean-sea ice-atmosphere system of the Hudson Bay Complex*. In *A Little Less Arctic*, S. H. Ferguson, L.L. Loseto, and M.L. Mallory, Eds., Springer, Netherlands, 1-38.

10. Population growth and aerosols in India

It is not surprising to commonly observe a correlation between decreasing air quality and increasing population in many countries. Data are needed, of course, to quantify such a correlation. Kishcha et al. did just this in a study of aerosol concentrations over India, and their Hall of Fame image showed the relationship between atmospheric aerosols and increasing human population on the Indian subcontinent. A particularly rainy year (2006-2007), shown by data from the Global Precipitation Climatology Project, resulted in a year with lower aerosols overall. Higher population densities were directly related to higher atmospheric aerosol concentrations.

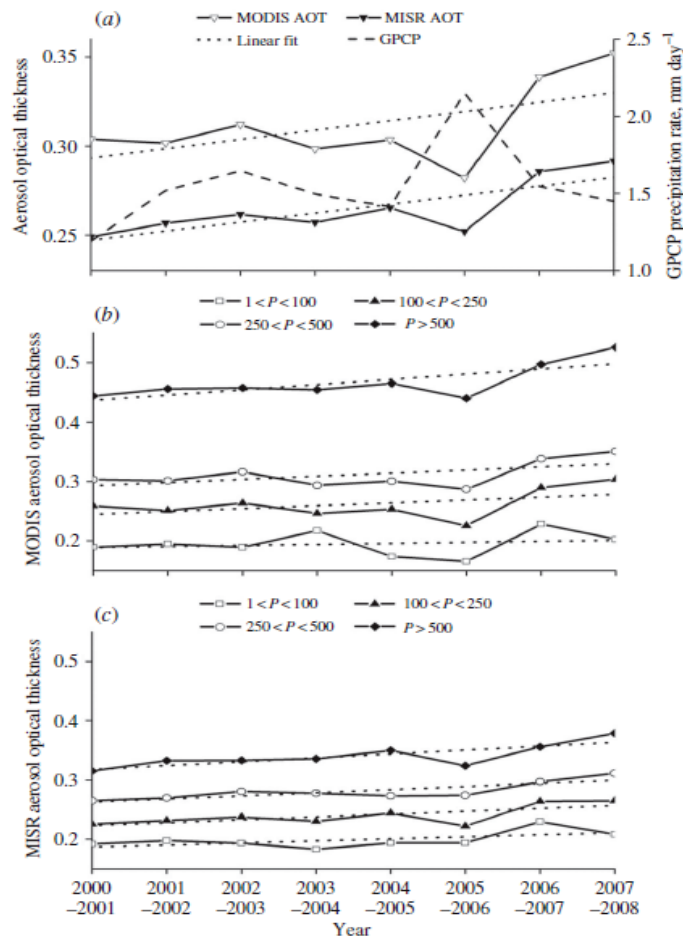


Figure 4. (a) The time series of aerosol optical thickness (AOT) averaged over the Indian subcontinent where $P > 1$ person km^{-2} for the months from October to February during the whole period under consideration (2000–2008), based on Moderate Resolution Imaging Spectroradiometer (MODIS) and Multiangle Imaging SpectroRadiometer (MISR) data. The dashed line designates the time series of GPCP precipitation rate averaged for the same months over the Indian subcontinent. (b) and (c) The time series of AOT averaged for the months from October to February over the regions with differing population densities (persons km^{-2}) (solid lines), based on (b) MODIS and (c) MISR data. The dotted lines designate linear trends.

Kishcha, P., Starobinets, B., Kalashnikova, O., and Alpert, P. (2011). Aerosol optical thickness trends and population growth in the Indian subcontinent. *International Journal of Remote Sensing*, 13 pp., doi:10.1080/01431161.2010.550333

11. Mineral dust aerosols over northern Africa

The development of an accurate model requires both accurate input data and a way to check the results of the model. Schmechtig et al. used Giovanni extensively in their analysis of the CHIMERE-DUST model accuracy for the annual cycle of dust in northern Africa. Three aerosol data products were used: OMI UV Aerosol Index, MODIS AOD, and Deep Blue AOD. (Deep Blue AOD provides AOD data over bright reflective surfaces (like desert sands and rocks)). The Hall of Fame image depicts the OMI UV Aerosol Index with an effective palette, showing the high concentrations associated with dust transport from the Bodélé Depression, a major source of atmospheric dust. Dust concentrations collected at the surface for the African Monsoon Multidisciplinary Analysis (AMMA) program and AERONET optical measurements were also used as inputs to the model.

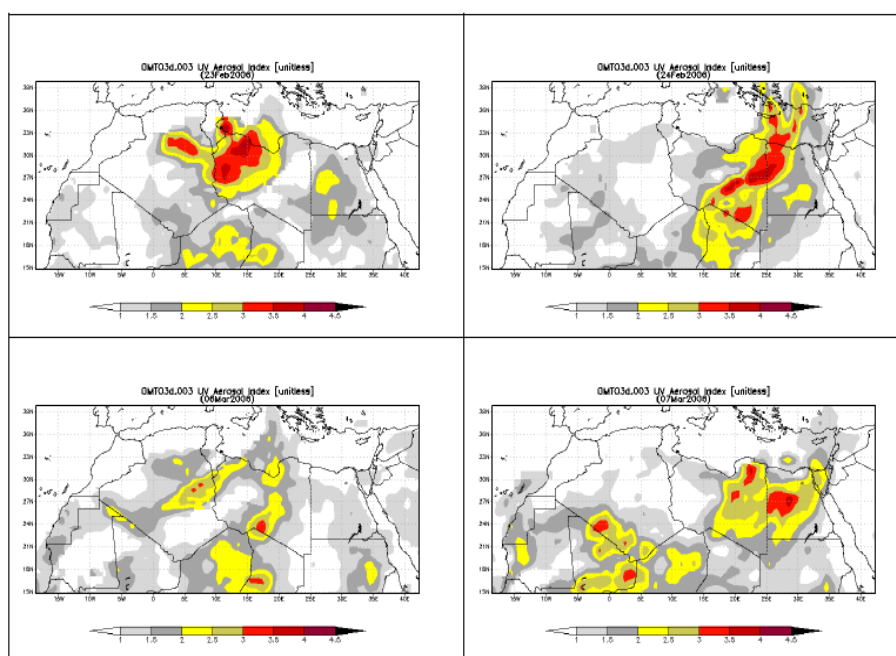


Fig. 7. Daily aerosol UV indexes derived from OMI satellite observations for 23 and 24 February 2006 (up) and for 6 and 7 March 2009 (down).

Schmechtig, C., Marticorena, B., Chatenet, B., Bergametti, G., Rajot, J. L., and Coman, A. (2011). Simulation of the mineral dust content over Western Africa from the event to the annual scale with the CHIMERE-DUST model. *Atmospheric Chemistry and Physics*, **11**, 7185-7207.

12.

The (brief) greening of Beijing

The smoggy atmosphere over China is well-known, and it is an increasing concern for both the people of China and the nations of the world. The government of China has attempted in various ways to deal with this particularly vexing environmental and public health problem, which results from a rapidly-growing economy, a reliance on coal for energy production, climate and weather patterns, and the topography of the country. Air quality conditions in Beijing were of particular concern to the international community of athletes, when Beijing hosted the Summer Olympics in 2008. In response, the government reduced automobile commuting, required areas around the city to reduce their industrial activities (and thus their emissions), and even stopped all construction activities in the city. Another initiative was to plant millions of plants and bushes, starting in 2001, to beautify the host city.

Regarding the aerosols, the athletes were lucky; weather patterns apparently kept the highest concentrations of aerosols just far enough from the city to make a difference. The improved air quality helped contribute to the success of the Olympics and the comfort and competitive abilities of the athletes. A side effect was that the clearer skies might have augmented the growth of the new trees and bushes, as indicated by the values of the Enhanced Vegetation Index (EVI) and the Normalized Difference Vegetation Index (NDVI), averaged over the June-August period using Giovanni. Jacquelyn Witte and her co-authors created this Hall of Fame image, documenting the increasing greenness in Beijing leading up to the Olympic year and the subsequent slight decline.

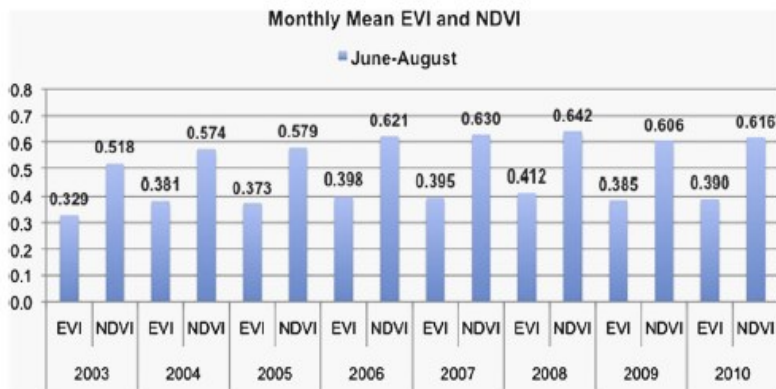


Fig. 6 June–August MODIS NDVI and EVI mean indices computed by the NASA GES DISC. The means are plotted per year between 2003 and 2010. The average of the Aqua and Terra V005 MODIS NDVI and EVI 3-month averages are shown. The area average encompasses the Beijing provincial borders and vicinity from 38–41°N to 115–118°E.

Witte, J.C., Duncan, B.N., Douglass, A.R., Kurosu, T.P., Chance, K., and Retscher, C. (2011). The unique OMI HCHO/NO2 feature during the 2008 Beijing Olympics: Implications for ozone production sensitivity. *Atmospheric Environment*, **45(18)**, 3103-3111, doi: 10.1016/j.atmosenv.2011.03.015.